Cellular Oncology (2025) 48:725–741
https://doi.org/10.1007/s13402-025-01043-y

RESEARCH

Meningeal leukaemic aggregates as foci of cell expansion and chemoresistance in acute lymphoblastic leukaemia metastasis

Paula Ortiz-Sánchez[1] · Sara González-Soto[1,2] · Luz H. Villamizar[1] · Jaris Valencia[1,3] · Eva Jiménez[1,3] · Rosa Sacedón[1,3] · Manuel Ramírez[4,5] · Isabel Fariñas[6] · Alberto Varas[1,3] · Lidia M. Fernández-Sevilla[3,7] · Ángeles Vicente[1,2]

Accepted: 30 January 2025 / Published online: 12 February 2025

Abstract

Purpose Central nervous system (CNS) involvement and/or relapse remains one of the most important causes of morbidity/mortality in paediatric B-cell precursor acute lymphoblastic leukaemia (BCP-ALL) patients. To identify novel therapeutic targets and develop less aggressive therapies, a better understanding of the cellular and molecular microenvironment in leptomeningeal metastases is key. Here, we aimed to investigate the formation of metastatic leptomeningeal aggregates and their relevance to the expansion, survival and chemoresistance acquisition of leukaemia cells.

Methods We used BCP-ALL xenograft mouse models, combined with immunohistofluorescence and flow cytometry, to study the development of CNS metastasis and the contribution of leptomeningeal cells to the organisation of leukaemic aggregates. To in vitro mimic the CNS metastasis, we established co-cultures of three-dimensional (3D) ALL cell spheroids and human leptomeningeal cells (hLMCs) and studied the effects on gene expression, proliferation, cytokine production, and chemoresistance.

Results In xenografted mice, ALL cells infiltrated the CNS at an early stage and, after crossing an ER-TR7$^+$ fibroblast-like meningeal cell layer, they proliferated extensively and formed large vascularised leukaemic aggregates supported by a network of podoplanin$^+$ leptomeningeal cells. In leukaemia spheroid-hLMC co-cultures, unlike conventional 2D co-cultures, meningeal cells strongly promoted the proliferation of leukaemic cells and generated a pro-inflammatory microenvironment. Furthermore, in 3D cell aggregates, leukaemic cells also developed chemoresistance, at least in part due to ABC transporter up-regulation.

Conclusion Our results provide evidence for the formation of metastatic ALL-leptomeningeal cell aggregates, their pro-inflammatory profile and their contribution to leukaemic cell expansion, survival and chemoresistance in the CNS.

Keywords Acute lymphoblastic leukaemia · Meningeal cells · Cell expansion · Chemoresistance · Central nervous system · 3D cell spheroids

1 Introduction

The central nervous system (CNS) is a key site of extramedullary disease in paediatric B cell precursor acute lymphoblastic leukaemia (BCP-ALL). Although CNS infiltration is rarely detected at diagnosis, data from clinical and post-mortem studies as well as from xenograft animal models suggest that CNS infiltration is an almost universal feature of ALL blasts, and its successful eradication is essential for long-term remission [1, 2]. Indeed, CNS involvement, especially relapse, remains one of the major challenges in paediatric oncology due to low cure rates and long-term treatment-related adverse effects, including acute and chronic neurotoxic sequelae [3, 4].

Ángeles Vicente and Lidia M Fernández-Sevilla contributed equally.

Ángeles Vicente is the first corresponding author, Lidia M Fernández-Sevilla is the second corresponding author and Alberto Varas is the third corresponding author.

Extended author information available on the last page of the article

The meninges are three fibrous sheaths that surround the brain and spinal cord: the dura mater, which is closer to the skull; the arachnoid membrane; and the pia mater, which is adjacent to the nerve tissue [5]. The arachnoid and pia mater, known as the leptomeninges, are separated by the subarachnoid space (SAS), a narrow space through which cerebrospinal fluid (CSF) flows, and have a unique molecular microarchitecture that is now starting to be unravelled [6–8]. The meninges have an essential structural and protective role in maintaining CNS homeostasis. Recent findings have revealed that they also provide a suitable microenvironment for the survival of a rich repertoire of myeloid and B cells which act, at steady state, as resident immune sentinels at the CNS border and recruit new immune cells from the calvarial bone marrow during brain insults [5, 9, 10]. Furthermore, the meninges have been described to play an important role in the immune responses that can affect the CNS during acute and chronic neuroinflammatory processes which occur in the context of acute injuries, viral infection and autoimmunity [11–16].

CNS leukaemia has been described primarily as a meningeal disease involving the dura mater and mainly the leptomeninges [2, 17]. Leptomeningeal infiltration by ALL cells can be seen as diffuse over brain surface or more often as isolated or multifocal nodules, separated from the brain parenchyma by an intact pial glial membrane [2, 17]. Although the formation of these meningeal leukaemic aggregates was already noted in the first post-mortem studies of ALL patients in the 1970s, no analysis of their characteristics or involvement in CNS leukaemia has been carried out to date. Similar compact leptomeningeal nodules attached to the brain surface have also been described in animal models of breast cancer brain metastasis suggesting their relevance in the development of the disease [18].

On the other hand, many studies have shown that the interactions between ALL cells and components of the bone marrow microenvironment play a pivotal role in the development, maintenance and chemoresistance of leukaemia [19, 20]. However, the role of the interactions between BCP-ALL cells and leptomeningeal cells, one of the most abundant stromal cell types which leukaemic cells find when they infiltrate the meninges, has been less investigated. The co-culture of leukaemia and meningeal cells in two-dimensional (2D) suspension cultures has been shown to promote the development of ALL chemoresistance [21, 22]. Using the same conventional 2D co-cultures, Jonart and collaborators [23] also reported that the contact with meningeal cells induces a reduction of the leukaemia proliferation rate. In xenograft mouse model studies, the analysis of leukaemia cell viability showed that leukaemic cells isolated from the meninges exhibit a higher viability that those found floating in the CSF [22]. Likewise, the treatment with compounds that disrupt the interactions between leukaemia and meningeal cells, reduces leukaemic CNS engraftment and improves the efficacy of the treatment with a chemotherapy drug alone [23, 24].

In the present study, we have conducted both in vivo xenograft mouse models and in vitro three-dimensional (3D) cell culture approaches with leukaemic cell spheroids and leptomeningeal cells to analyse the dynamics of meningeal leukaemic aggregate formation, their relevance for the dissemination and chemoresistance of leukaemic cells in the CNS, and the involvement of leptomeningeal cells in this metastasis.

2 Materials and methods

2.1 Cell lines

BCP-ALL cell lines Nalm6 (ACC128) and RS4;11 (ACC508) were purchased from DSMZ (German Collections of Microorganisms and Cell Cultures) and cultured in RPMI 1640 supplemented with 10% foetal bovine serum (FBS), 2 mM L-glutamine, and penicillin/streptomycin (all from Lonza, Basel, Switzerland).

Human leptomeningeal cells (hLMCs; ScienCell Research Laboratories, Carlsbad, CA, USA) were immortalised by Innoprot (Bizkaia, Spain; P10352-IM) and maintained in Meningeal Cell Medium (MenCM, Innoprot; P60113) supplemented with 2% FBS and growth factors according to supplier's recommendations.

2.2 BCP-ALL xenograft model

NOD.Cg-Prkdc scid IL2rg tm1Wjl/SzJ (NSG) male mice were purchased from The Jackson Laboratories (Bar Harbor, ME, USA) and housed under pathogen-free conditions. All animal experimentation was conducted in accordance with the Spanish guidelines for care and use of laboratory animals and protocols approved by the Complutense University and Community of Madrid (PROEX 015/19; PROEX 204.2/22). Eight- to twelve-week-old mice were IV-infused via the tail vein with $0.5\text{-}5 \times 10^6$ BCP-ALL Nalm6, RS4;11 or primary cells. Three primary samples were obtained from marrow aspirates of BCP-ALL patients and used where indicated. These samples were provided by the Onco-Haematology Unit at Niño Jesús University Children's Hospital and the study approved by the Ethics Committee of Clinical Research at the Hospital (R-0009/22). Mice were anesthetised and euthanised at different time points (7, 14 and 21 days after Nalm6 cells infusion; 7, 14, 21, 28 and 35 days after RS4;11 cells injection; and 14, 21, 42 and 63 days after primary BCP-ALL cells injection) or when they

showed evident disease symptoms (rough hair, lethargy, hunched-back posture, loss of motor functions, hyperventilation, hind limb paralysis). Brains were then obtained and processed for histological studies or thoroughly washed with PBS containing 1% EDTA to collect the leukaemic cells accumulated in the SAS. Spleens were also removed and dissociated in a 40 µm cell strainer by using the rubber plunger of a 1 ml syringe to obtain a single cell suspension. All cell suspensions were then processed for flow cytometry analysis.

2.3 Tissue immunofluorescence and histological analysis

For tissue immunofluorescence studies, brains were directly embedded in OCT compound (Thermo Fisher Scientific, Waltham, MA, USA), frozen rapidly and stored at −80 °C until cryostat sectioning. Brain sections (10 µm thick) were first blocked in PBS with 5% normal donkey serum followed by incubation with the following primary antibodies: anti-hCD19 (Immunostep, Salamanca, Spain; 19PU1-01MG) 1:100; anti-laminin (Merck KGaA, Darmstadt, Germany; L9393) 1:300; anti-ER-TR7 (Santa Cruz Biotechnology, Santa Cruz, CA, USA; sc-73355) 1:50; anti-podoplanin (Clone PA2.26, kindly provided by Dr. Martín-Villar´s lab [25]) 1:100; anti-mCD31 (BD Biosciences, San Jose, CA, USA; 550274) 1:100; and anti-Ki67 (Abcam, Cambridge, UK; ab15580) 1:150, in 10% bovine serum albumin (BSA) in PBS for one hour at room temperature. After washing three times with PBS, sections were then incubated with the appropriate Alexa Fluor-conjugated secondary antibodies (Thermo Fisher Scientific) for 45 min. Sections were then washed, and nuclei were counterstained with DAPI. Samples were mounted with Prolong Gold (Thermo Fisher Scientific; P10144) and examined using a Nikon Eclipse Ci fluorescence microscope. Image acquisition was performed using Nikon Digital sight DS-U3 and Nis-Elements D viewer software. Finally, Fiji software was used for image processing.

For histological analysis, brain samples were fixed by immersion in 4% glutaraldehyde, buffered to pH 7.3 with Millonig's fluid, post-fixed in 1% osmium tetroxide in the same buffer, and dehydrated in acetone for embedding in Araldite (Merck KGaA). Semithin sections (0.5 µm thick) were obtained using an OM-U3 ultramicrotome (Reichert, Vienna, Austria), stained with toluidine blue and mounted with Canada balsam mounting medium (Merck KGaA; C1795) to preserve the samples.

2.4 Cell cultures

For 2D cultures, 4×10^4 hLMCs were seeded in 24-well plates previously coated with Geltrex™ basement membrane matrix (150 µg/ml; Thermo Fisher Scientific; A1413202). Following overnight adherence, leukaemic cells were added at a 1:5 ratio for 72 h. The culture media used for these co-cultures was a mixture of leukaemic cell and hLMCs media without growth factors in a 1:2 ratio with 2% FBS. Leukaemic cells were collected in two steps. First, non-adherent cells were obtained by collecting the media containing floating leukaemic cells and washing the cultures with 5 mM EDTA-PBS. Then, treatment with TrypLE™ Express enzyme solution (Thermo Fisher Scientific; 12604039) was used to collect those cells firmly adhered to hLMCs. Image acquisition of cell cultures was performed using a Nikon Digital Sight DS-Fi1 camera.

For 3D cultures, Nalm6 or RS4;11 cells were embedded in Geltrex and seeded as droplets of 50 µl (0.5×10^5 cells per droplet) in 24-well plates with untreated surface. Drops were allowed to solidify for 20 min at 37 °C and then culture medium was added. Co-cultures of leukaemic spheroids and hLMCs were performed by placing the spheroids on hLMC monolayers in RPMI and MenCM (1:2 ratio) with 2% FBS and without growth factors. After 8 days of co-culture, supernatants were collected, and proliferation assays were performed. For cell counting and flow cytometry analysis, cells embedded in Geltrex were recovered by using Corning™ Cell Recovery Solution (Thermo Fisher Scientific; 354253). For gene expression analysis, leukaemic cells were isolated by using magnetic beads following the supplier's instructions. Briefly, cell suspensions were incubated with biotinylated anti-hCD19 monoclonal antibody (BioLegend; 302203) for 30 min and $CD19^+$ cells were positively isolated with Dynabeads™ Biotin Binder (Thermo Fisher Scientific; 11047) using the DynaMag™ Spin Magnet (Thermo Fisher Scientific; 12320D).

2.5 Cytokine measurements

Production of different cytokines and chemokines was measured in supernatants from leukaemic spheroids, hLMCs and ALL spheroids-hLMCs co-cultures by using LEGENDplex™ HU Essential Immune Response Panel and LEGENDplex™ Human Inflammation Panel 2 (BioLegend), following the manufacturer's recommendations.

2.6 Immunocytofluorescence

Standard 2D cell cultures were fixed with 4% paraformaldehyde in PBS, permeabilised in PBS with 0.05% saponin and blocked in PBS 10% FBS. Next, cells were labelled with

anti-hCD19 and anti-Ki67 antibodies for one hour, washed three times with PBS and then incubated with the appropriate Alexa Fluor-conjugated secondary antibodies and Phalloidin DyLight™ 594 (Thermo Fisher Scientific; 21836) for one hour at room temperature. Cell nuclei were stained with DAPI, and samples were mounted with ProLong Gold antifade reagent.

For 3D culture studies, leukaemic spheroids and hLMCs co-cultures were carried out on 10 mm diameter glass coverslips. Immunofluorescence was performed by blocking and permeabilising samples in PBS containing 0.3% Triton-X and 2% BSA for 2 h at room temperature. Cells were then washed with PBS containing 0.1% Triton-X and 0.05% BSA and incubated with anti-hCD19 or anti-Ki67 antibodies diluted in the same solution overnight at 4 °C. After washing three times, samples were incubated with the appropriate Alexa Fluor-conjugated secondary antibodies for two hours at room temperature. When indicated, cells were stained with Phalloidin DyLight™ 594. DAPI was used for nuclear counterstaining. Coverslips were mounted on Superfrost Plus slides with FluorSave Reagent (Merck KGaA; 345789). Samples were photographed in an Olympus FluoView FV10i confocal microscope and images were processed with Fiji software.

2.7 Proliferation and viability assays

To study cell proliferation, cell suspensions obtained from xenograft mouse spleen and SAS or cells harvested from cultures were fixed and permeabilised with 70% ethanol. After several washes in PBS, 7-amino-actinomycin D (7-AAD; Merck KGaA) was added and the cell cycle analysed using flow cytometry. Intracellular Ki67 staining was also analysed by flow cytometry to study cell proliferation. For the analysis of immunofluorescence images of 3D co-cultures with Ki67/DAPI staining, regions of interest (ROIs) were selected and leukaemic nuclei were segmented based on DAPI staining using the FiJi plugin StarDist. Then, fluorescence intensity of Ki67 staining was quantified in each cell. Cells with an intensity value higher than the median of all nuclei were considered $Ki67^+$ cells. The percentage of $Ki67^+$ cells was calculated in each condition by quantifying 9–13 fields and 400–700 cells.

For cell viability analysis, 2D and 3D cell cultures were treated, where indicated, with or without 1 μM methotrexate (MTX; Pfizer, Nueva York, NY, EEUU) for 48 h. Cells were then stained either with trypan blue and counted with a haemocytometer, or with DY634-conjugated annexin V (Immunostep; ANXVDY-200T) and propidium iodide (BioLegend), in combination with anti-hCD19 antibodies (BioLegend), and analysed by flow cytometry. Viable cells were defined as propidium iodide- and annexin V-negative cells.

2.8 Flow cytometry

Before staining with specific antibodies, cells were incubated at 4 °C for 5 min with FcR Blocking Reagent (Miltenyi Biotec, Bergisch Gladbach, Germany; 130-059-901) to block nonspecific binding. Then, immunofluorescence stainings were carried out by incubating cells in the presence of saturating amounts of fluorochrome-conjugated antibodies for 30 min at 4 °C: anti-hCD19-FITC / -Alexa Fluor 647 (BioLegend; 302205 / 302222) 1:20; anti-mCD45-PE / Alexa Fluor 488 (BioLegend; 110708 / 103121) 1:10–20; anti-hCD44-FITC (BD Biosciences; 555478) 1:10; anti-hCD106/VCAM1-APC (BD Biosciences; 551147) 1:20; anti-hCD54/ICAM1-Alexa Fluor 488 (BioLegend; 322713) 1:10. For the intracellular detection of Ki67, cells were treated with BD FACS Permeabilizing Solution 2 (BD Biosciences; 347692), according to the manufacturer's instructions, and stained with anti-Ki67 for 30 min. Analyses were conducted in a FACSCalibur flow cytometer (BD Biosciences) at the Centro de Citometría y Microscopía de Fluorescencia (UCM) and analysed with FCS Express V3 software.

2.9 RT-PCR analysis

RNA was isolated using SpeedTools Total RNA Extraction kit (Biotools, Madrid, Spain; 21.212–4210) including a DNase digestion step, as recommended by the supplier, to avoid genomic DNA contamination. Total cDNA was synthesised with the High-Capacity cDNA Reverse Transcription Kit (Thermo Fisher Scientific; 4368814) according to the manufacturer's instructions, and real-time quantitative PCR was performed by using the following pre-designed Taqman assays obtained from Applied Biosystems (Thermo Fisher Scientific): *ABCA2* (Hs00242232_m1); *ABCA3* (Hs00184543_m1); *ABCC1* (Hs01561483_m1); *FN1* (Hs01549976_m1); *HSPG2* (Hs01078536_m1); *ICAM1* (HS00164932_m1); *ITGA4* (Hs00168433_m1); *ITGAL* (Hs00164957_m1); *LAMC1* (Hs00267056_m1). Amplifications, detections and analyses were performed in a 7.900HT Fast Real-time PCR System (Centro de Genómica, UCM). The ΔCt method was used for normalization to GNB2L1 mRNA.

2.10 Statistical analysis

Statistical comparisons between two experimental groups were performed using the parametric Student t-test or the non-parametric Mann-Whitney U test, as appropriate. Shapiro-Wilk test was used for assessing variable normality. Analyses were performed with the GraphPad Prism 8.0 software (GraphPad Inc, San Diego, CA, USA). Values of

$p \leq 0.05$ (*), $p \leq 0.01$ (**) and $p \leq 0.001$ (***) were considered to be statistically significant.

3 Results

3.1 Study of metastatic leukaemic aggregates in the leptomeninges

Both BCP-ALL cell lines (Nalm6 and RS4;11) and primary cells, when injected into NSG mice, were able to invade the CNS accumulating mainly in the SAS as leptomeningeal metastasis. The leukaemic infiltration appeared diffusely distributed over the brain surface or, more often, forming multifocal meningeal leukaemic aggregates tightly adhered to the pia mater, especially at the level of main brain fissures (Fig. 1A-F).

To know the kinetics of leptomeningeal metastases during leukaemia development, we first studied the evolution of tumour cell numbers in Nalm6-, RS4;11- and primary BCP-ALL cell-xenografted mice, in which the disease progressed differently, with Nalm6-injected mice showing more pronounced disease symptoms which developed significantly earlier than in RS4;11- and primary BCP-ALL cell-injected mice (Supplementary Fig. S1A-C). Flow cytometry studies indicated that the first leukaemic cells could be found in the SAS of Nalm6-mice at 2 weeks post-infusion, exponentially increasing their numbers in the following weeks (Fig. 1G, H). In contrast, and reflecting a slower development of the systemic disease, the detection of leukaemic cells in the SAS of RS4;11- and primary BCP-ALL-animals was delayed for one or several weeks, increased in subsequent weeks and reached significantly higher numbers of tumour cells than in Nalm6-animals by the end of the disease (Fig. 1G, H).

In parallel, the formation process of the meningeal leukaemic aggregates was studied in brain cryosections. When the first leukaemic cells were identified in the SAS, they appeared in close contact with a fibroblast-like cell layer, rich in matrix components, which rested on the pia mater and initially prevented the passage of leukaemia into deeper meningeal zones. Those meningeal fibroblast cells expressed the ER-TR7 antigen, a cell marker commonly used to identify the leptomeninges, mainly the arachnoid mater (Fig. 2A, D, G; Supplementary Fig. S2A, D) [8, 26]. During the first weeks, the space comprised between these two cell layers appeared to be largely collapsed and was only visible near the passageways of the cerebral arteries and veins (Fig. 2A). However, in more advanced stages of the disease, and particularly in the areas surrounding the major brain fissures, leukaemic cells broke through the ER-TR7$^+$ layer and progressively increased in number in the space defined by the pial vascular membrane and the ER-TR7$^+$ arachnoid layer, which also began to express laminin (Fig. 2B, E and H C, F, I; Supplementary Fig. S2B, E and S2C, F). Leukaemic cells then appeared to be organised in a reticular network of podoplanin (PDPN)-positive leptomeningeal cells, components of the extracellular matrix and small blood vessels mainly in the areas closest to the pia mater, giving rise to large and complex vascularised structures (Figs. 1B-D and 2J and K). The process of formation of these meningeal leukaemic cell complexes was similar in all xenografted mice used, although in the case of primary BCP-ALL- and RS4;11-injected mice they developed with a one or more-week delay and the size they reached at the end of the disease was significantly larger than those observed in Nalm6-mice, in correlation with the greater number of cells recovered from the SAS of the former (Fig. 1B-D, G, H).

3.2 Meningeal aggregates as potential sites of CNS metastatic spread

To elucidate whether meningeal aggregates could be formed by the massive infiltration of leukaemic cells from the skull bone marrow and/or by the proliferation of a discrete number of cells that reached the SAS, we assessed the proliferation rate of leukaemic cells during the course of the disease. Histological and immunofluorescence studies of Ki67 expression in brain sections from the xenografted mice revealed that, both in the early stages of aggregate formation and when they reached a significant size at the end of the disease, a large proportion of Nalm6/RS4;11 CD19$^+$ cells were positive for Ki67, even those leukaemic cells located in proximity to the pia mater (Fig. 3A-E). The proliferative rate of leukaemic cells present in the SAS was also quantified by flow cytometry using two different experimental strategies. As shown in Fig. 3F-G (and Supplementary Fig. S3A), the percentage of CD19$^+$ cycling cells ($S+G_2+M$ phases) or Ki67-positive cells recovered from the meninges of xenografted mice was high and similar to that found in other extramedullary tissues colonised by leukaemic cells during the course of the disease. Furthermore, the viability of leukaemic cells recovered from the CNS at the end of the disease was approximately 90% in all cases (Fig. 3H). Therefore, meningeal aggregates appear to represent areas where leukaemic cells could expand from a reduced number of infiltrating tumour cells.

On the other hand, the immunofluorescence study of the brain cryosections from xenograft mice revealed that, within the aggregates and located between the arachnoid layer previously defined as ER-TR7$^+$ and the pia mater, a discrete subpopulation of leukaemic cells exhibited low levels of CD19 expression (Fig. 3D; Supplementary Fig. S3B, C). To determine whether leukaemia attachment to leptomeningeal cells could promote CD19 downregulation,

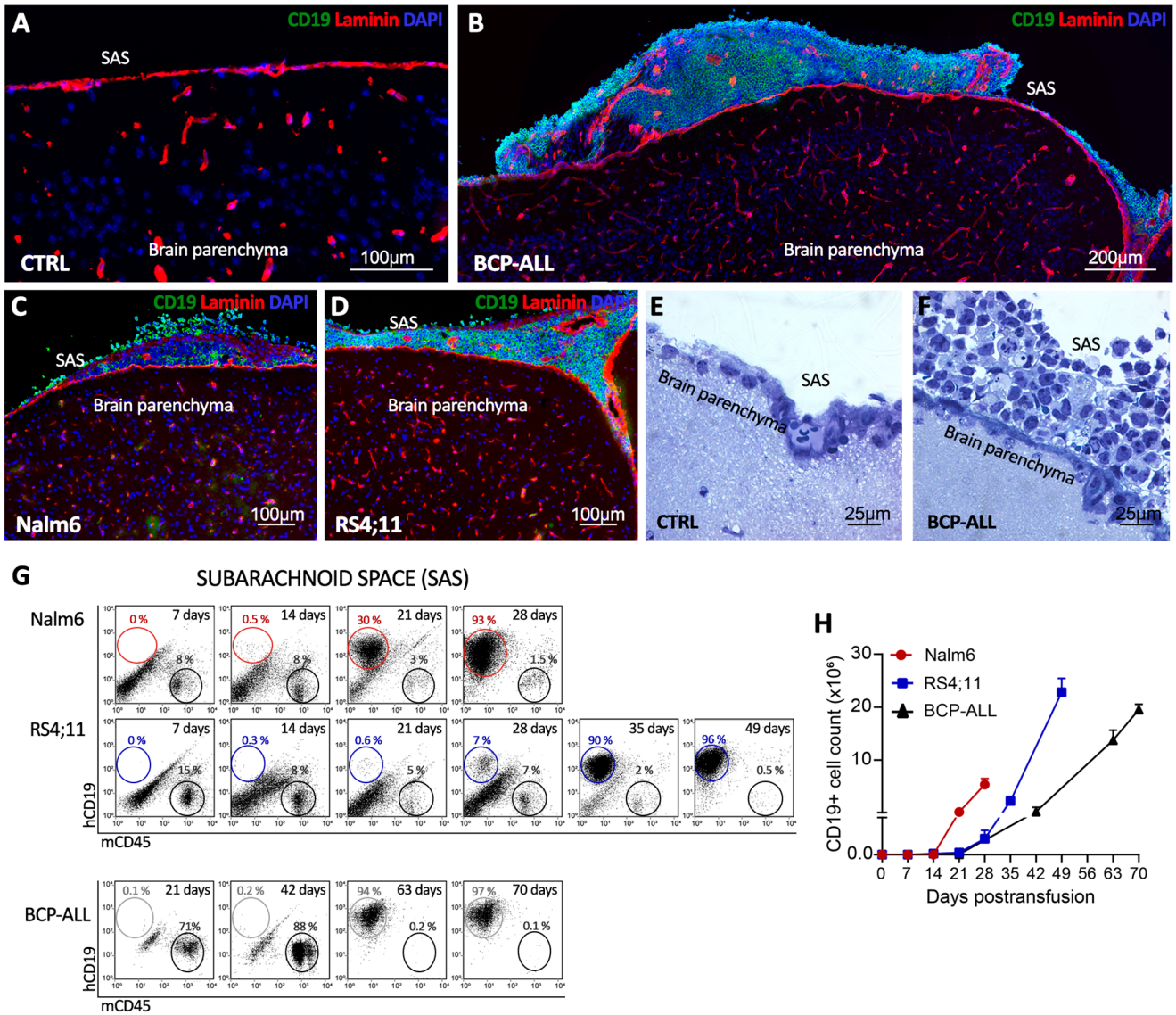

Fig. 1 Kinetics of leukaemic metastasis in the leptomeninges of BCP-ALL xenografted mice. **A-D** Representative images of CD19 (green) and laminin (red) expression in sagittal brain cryosections of healthy (**A**) and primary BCP-ALL- (**B**), Nalm6- (**C**), and RS4;11-injected mice (**D**) at the final stage of the disease. Note the large leukaemic aggregates closely attached to the brain surface near the longitudinal fissure (SAS, subarachnoid space). **E-F** Semi-thin brain sections stained with toluidine blue showing cortical brain in healthy (**E**) and primary BCP-ALL xenografted mice (**F**). **G** Average number of $CD19^+$ leukaemic cells (±SEM) found in the SAS of mice xenografted with BCP-ALL Nalm6, RS4;11 or primary cells at different times after cell transplantation ($n = 3–8$ mice/group). **H** Representative dot plots showing the percentage of human leukaemic cells ($hCD19^+$) and murine leukocytes ($mCD45^+$) present in the SAS at different times post-transplantation

the expression of this antigen was analysed in co-cultures of hLMCs with BCP-ALL cells (Fig. 4). Immunofluorescence images showed that a proportion of CD19-positive cells strongly adhered to hLMCs (Fig. 4A-C). Flow cytometry analysis of CD19 antigen expression in the non-adherent versus the adherent cell fraction revealed that CD19 expression was significantly lower in the latter (Fig. 4D, E), suggesting that the direct contact of leukaemic cells with hLMCs may favour downregulation of this antigen, which could consequently reduce the effectiveness of CAR-T cell therapies [27].

3.3 Leukaemia-leptomeningeal cell interactions promote BCP-ALL cell proliferation and a proinflammatory microenvironment

In order to study the potential advantages that the organisation of the meningeal aggregates could confer on tumour cells, we first developed a three-dimensional (3D) culture

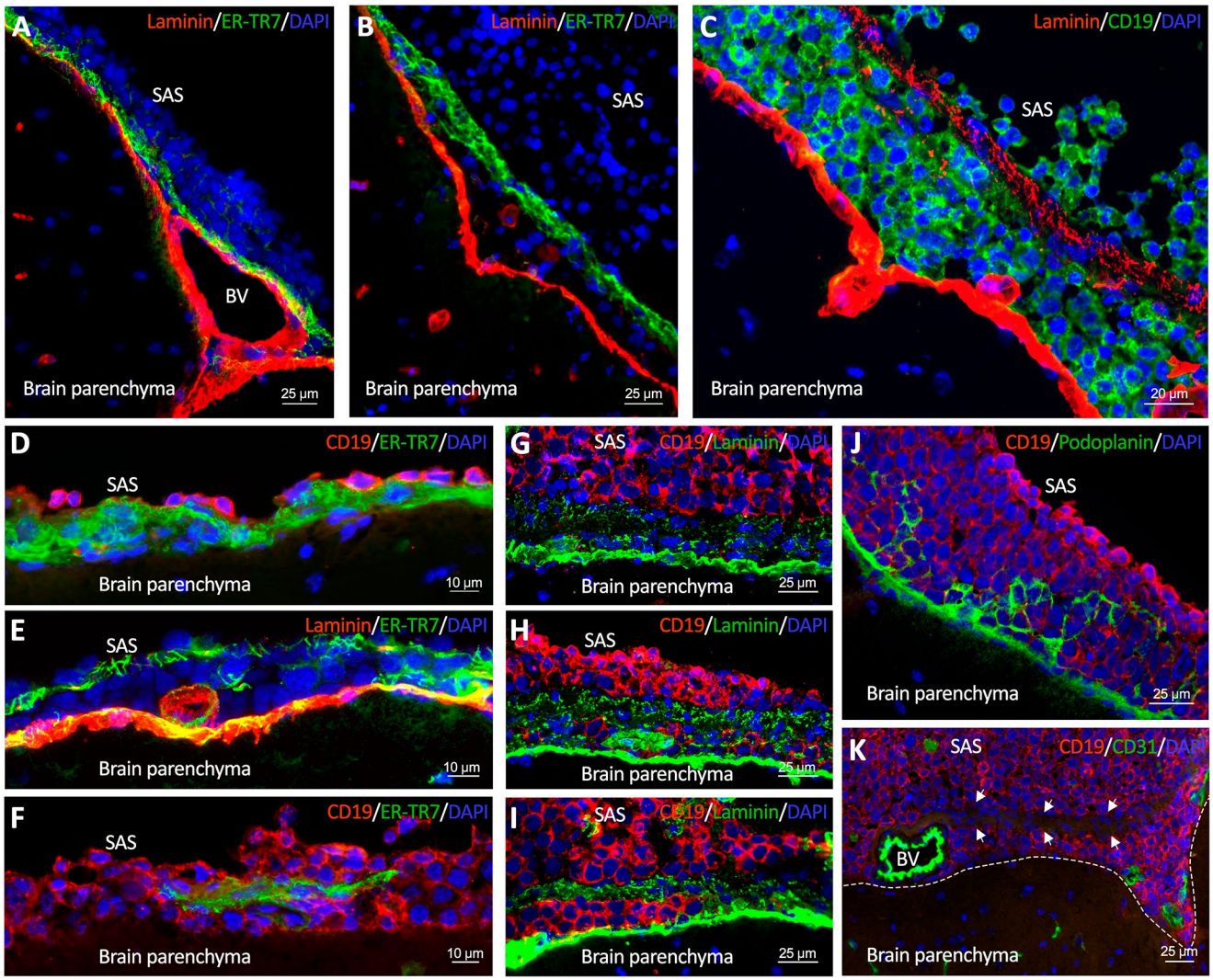

Fig. 2 Formation of leukaemic aggregates in the leptomeninges of mice xenografted with BCP-ALL cells. **A**, **D**, **G** Representative images of the early stages of the formation of leukaemic cell aggregates in the brain of Nalm6-injected mice. $CD19^+$ leukaemic blasts appear in close contact with fibroblast-like ER-$TR7^+$ cells. In the images the subarachnoid space (SAS) appears collapsed and the ER-$TR7^+$ cell layer is seen in contact with the $laminin^+$ pia mater (BV, blood vessel). **B**, **E**, **H** In intermediate stages, some isolated leukaemic cells are already located between the ER-$TR7^+$ arachnoid layer and the pial-glial barrier. **C**, **F**, **I** In more advanced stages, leukaemia cells accumulate between the ER-$TR7^+$ $laminin^+$ leptomeningeal layer and the pial-glial barrier. **J** $Podoplanin^+$ leptomeningeal cell network extending from the pia mater into a leukaemia cell aggregate. **K** $CD19^+$ leukaemic aggregate with $CD31^+$ blood vessels located between the inner arachnoid layer (arrows) and the pia mater. Images shown are representative of 3–5 mice per group

system of leukaemia cells, that mimics the aggregates observed in the in vivo model, and analysed various aspects of the tumour cells there confined. As shown in Fig. 5, BCP-ALL cells organised in 3D spheroids exhibited an increased expression of the extracellular matrix components *LAMC1* (laminin), *FN1* (fibronectin) and *HSPG2* (heparan sulphate proteoglycan) as well as the adhesion molecules *ITGAL* (LFA-1), *ICAM1* and *ITGA4* (VLA-4), compared to the cells cultured in suspension.

The higher expression of integrins and heparan sulphate proteoglycans observed in leukaemia cell aggregates may favour their adhesion to meningeal cells, which express their partner receptors (Supplementary Fig. S4). Therefore, to know the effect of leukaemia-hLMC interactions on tumour cell expansion and maintenance, we modelled the leptomeningeal leukaemic metastasis by culturing the BCP-ALL cell spheroids on a layer of hLMCs (Fig. 6). After 96 h of co-culture, areas of close contact between leukaemic and meningeal cells were observed, both by migration of the former towards the edges of the spheroids and by entry of meningeal cells into the leukaemic aggregates (in control cultures, without the presence of leukaemic cells, hLMCs were not attracted to the acellular spheroids, which eventually lost their integrity). These interactions increased

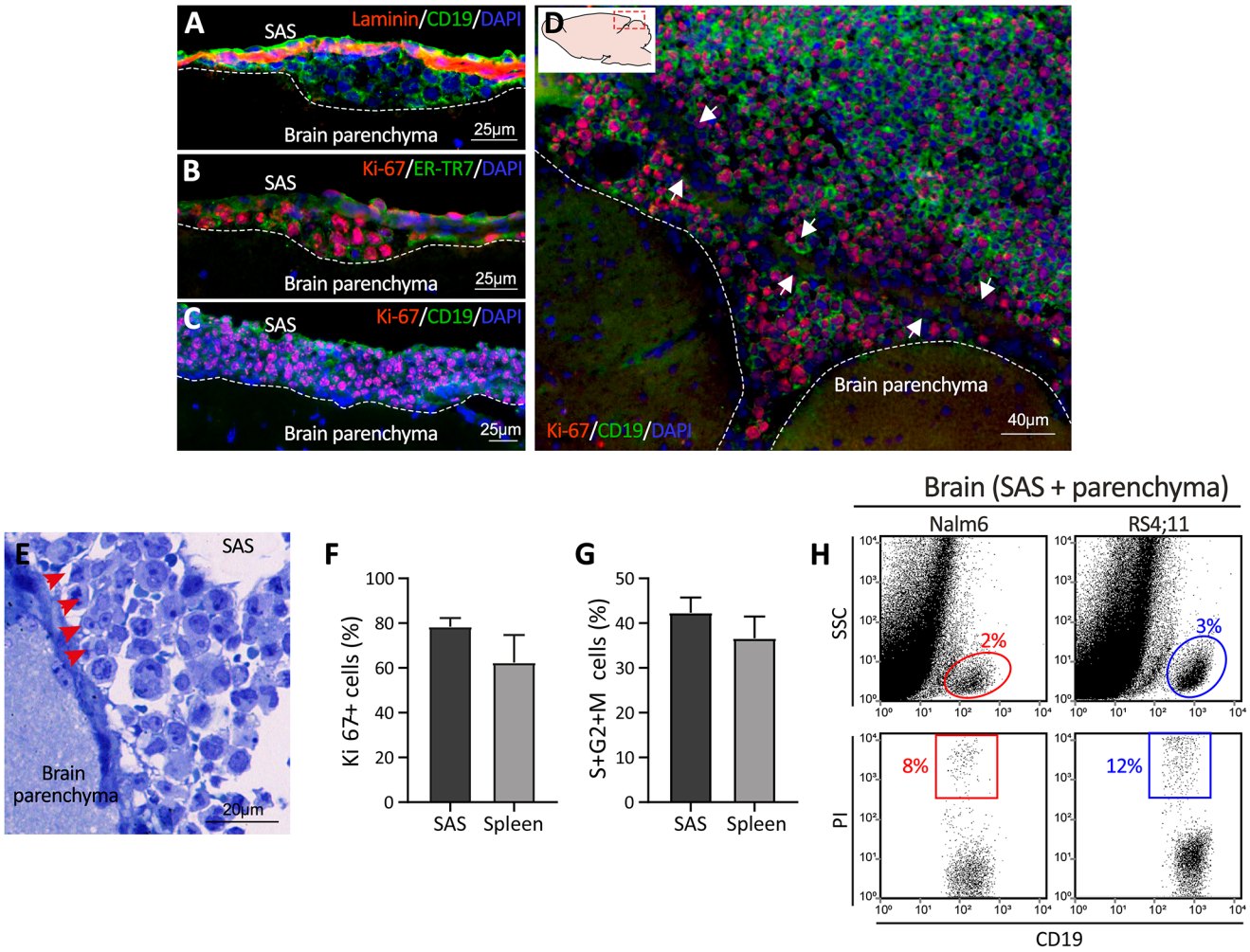

Fig. 3 Proliferation of leukaemic cells in leptomeningeal aggregates. **A-B** $CD19^+$ $Ki67^+$ proliferating leukaemic cells located between the $ERTR7^+$ layer and the pia mater in Nalm6-injected mice 21 days post-infusion. **C** $Ki67^+$ proliferating RS4;11 leukaemic cells 35 days after transplantation. Note the Ki67 positivity of the cells regardless of their distance to the pia mater. **D** Large aggregate of $CD19^+$ leukaemic cells in the leptomeninges of Nalm6-mice at the end of the disease where abundant $Ki67^+$ proliferating cells are observed. Leukaemic cells located between the pia mater (close to brain parenchyma) and the inner arachnoid layer show a lower CD19 expression on their surface (green staining). Arrows define the inner arachnoid layer. **E** Toluidine blue-stained semi-thin section of a leukaemic aggregate in SAS of Nalm6-injected mice showing blasts in different phases of mitosis (red arrowheads) and in close contact with the pia mater. (**A-E**) Images are representative of 3–5 mice per group. **F** Bars represent mean (±SEM) of $CD19^+Ki67^+$ cells measured by flow cytometry in the SAS and spleen of Nalm6-mice at the end of the disease ($n=3$–4). **G** Bars represent mean (±SEM) of $CD19^+$ leukaemic cells in $S+G_2+M$ cell cycle phases in the SAS and spleen of Nalm6-mice at the end of the disease ($n=3$–6). **H** Representative dot plots showing the percentage of propidium iodide (PI^+) cells within the population of $CD19^+$ leukaemic cells recovered from whole brains of Nalm6- and RS4;11-injected mice at 28 days and 49 days post-infusion, respectively

significantly over the following days of culture, revealing the mutual attraction between leukaemia and leptomeningeal cells, and in parallel a strong increase in the number of leukaemic cells was also observed (Fig. 6A; Supplementary Fig. S5). So, the role of leptomeningeal cells as inducers of leukaemic proliferation in the 3D leukaemia-hLMC cocultures was next evaluated. As shown in Fig. 6B, after 8 days of co-culture, the numbers of $CD19^+$ BCP-ALL cells were significantly higher in the presence of leptomeningeal cells compared to those recovered from control spheroids without hLMCs. No differences were observed in the viability of leukaemia cells harvested from both types of cultures (Fig. 6C). Consistent with these results, the percentage of $Ki67^+$ leukaemic cells in the control spheroids ranged from 15 to 20%, whereas in those cultured in the presence of hLMCs, RS4;11- and Nalm6-$Ki67^+$ cells reached values of 50 and 65%, respectively (Fig. 6D, E). These results were confirmed by flow cytometry studies showing that the percentage of cycling leukaemic cells was significantly higher in the spheroids grown in the presence of hLMCs (Fig. 6F). However, and strikingly, the presence of leptomeningeal cells in conventional 2D co-cultures either significantly

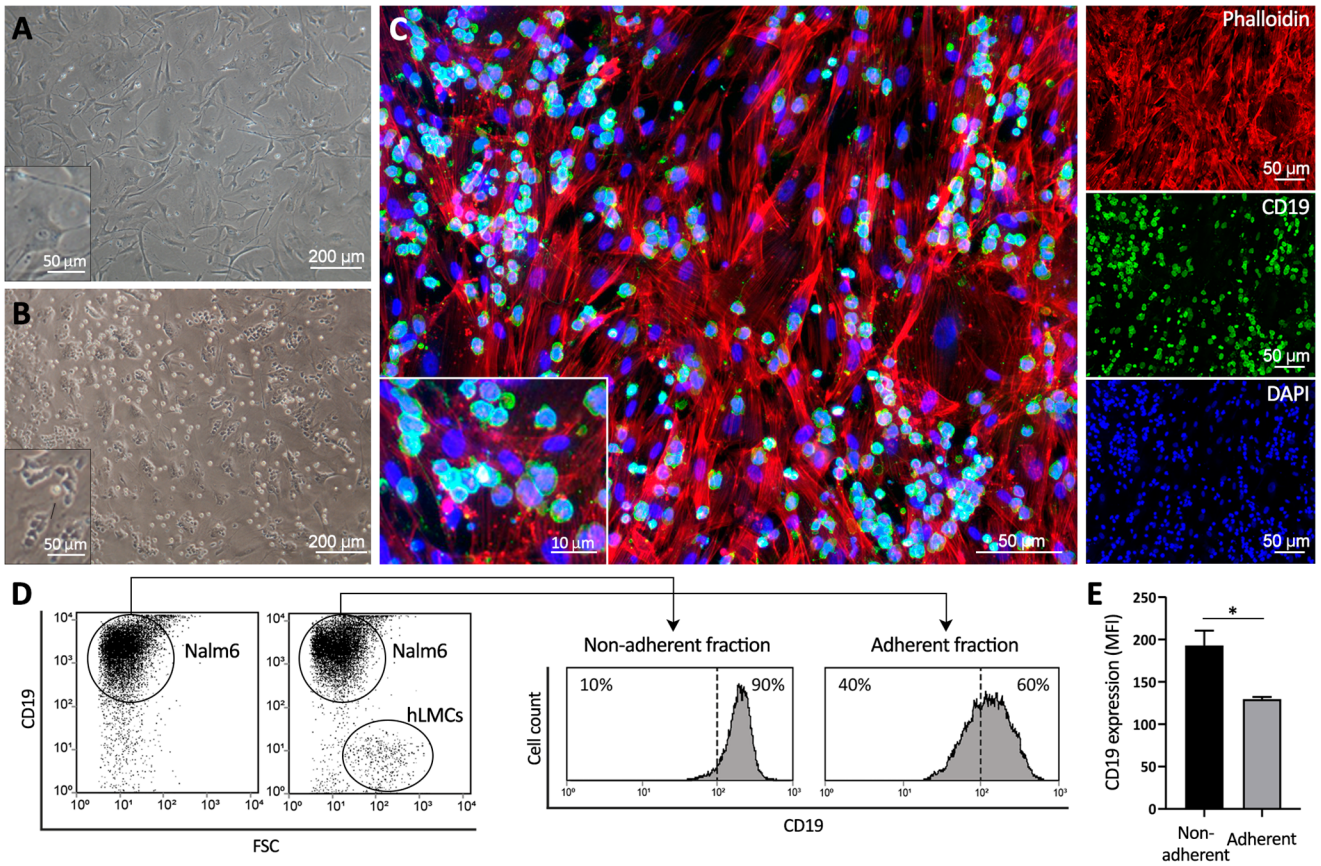

Fig. 4 Leukaemic cells downregulate CD19 expression after contact with leptomeningeal cells. **A**-**B** Representative images of human leptomeningeal cells (hLMCs) cultured for 72 h alone (**A**) or with Nalm6 leukaemia blasts (**B**). **C** Immunofluorescence images of $CD19^{+}$ Nalm6 blasts co-cultured with hLMCs showing their typical fibroblastic appearance as revealed by phalloidin labelling. The detail shows two populations of leukaemic cells differentiated by their size and CD19 expression. **D** Representative flow cytometry histograms showing CD19 expression in adherent and non-adherent leukaemic cells recovered from hLMC co-cultures. In each case, the percentage of $CD19^{high}$ and $CD19^{low}$ positive cells is indicated. **E** Bars represent the mean fluorescence intensity (MFI) of CD19 (mean ± SEM of four independent experiments) in the non-adherent and adherent leukaemic cell populations. (*$p \leq 0.05$, Student t test)

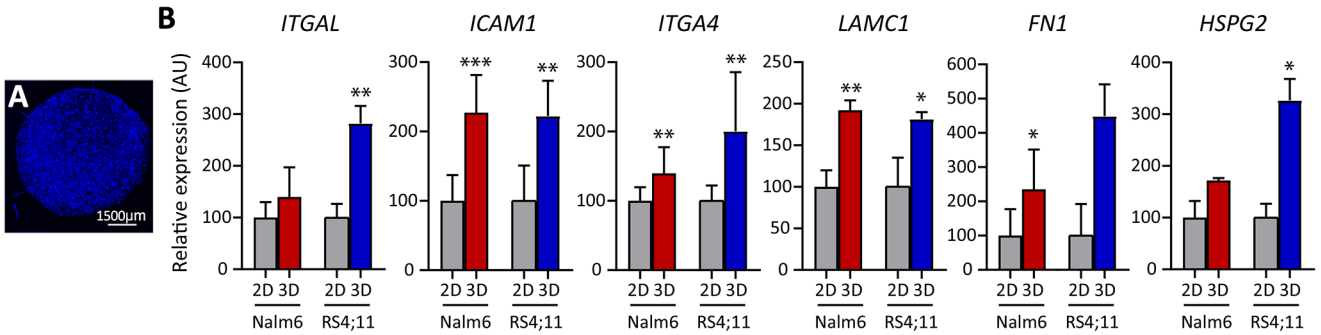

Fig. 5 Changes in the expression of extracellular matrix and adhesion molecules in leukaemic spheroids mimicking in vivo leptomeningeal metastasis. **A** Confocal image of a 3D spheroid containing DAPI-labelled ALL cells. **B** RT-qPCR quantification of mRNA levels for various adhesion molecules and extracellular matrix components in BCP-ALL cells (Nalm6, red and RS4;11, blue) cultured in 3D spheroids relative to their expression in 2D suspension cultures. Bars show mean ± SEM of $n=8$ and $n=4$ independent experiments with Nalm6 and RS4;11 cells, respectively. (*$p \leq 0.05$, **$p \leq 0.01$, ***$p \leq 0.001$; Mann–Whitney U test)

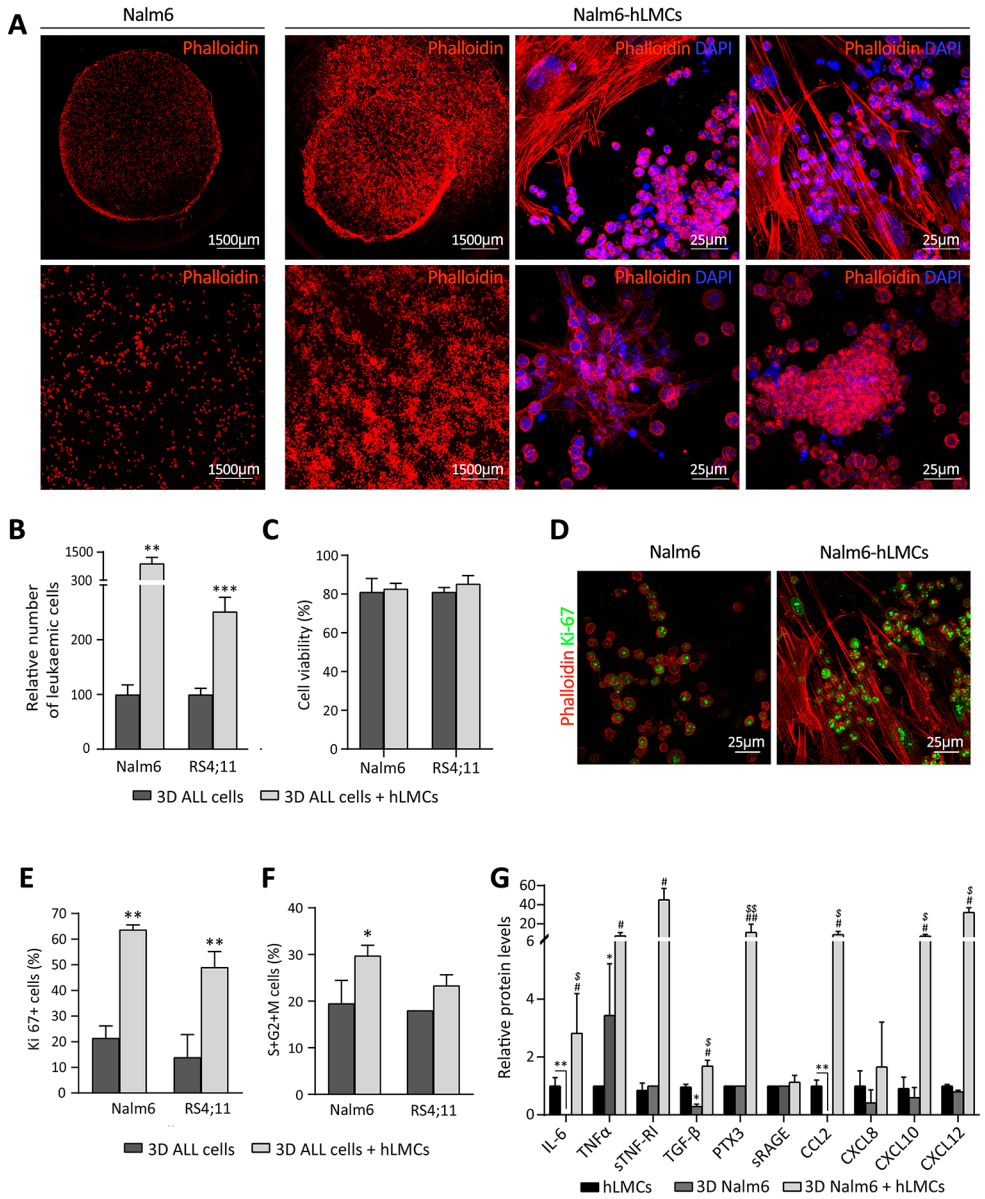

Fig. 6 Co-culture of 3D leukaemic spheroids and leptomeningeal cells stimulate the secretion of pro-inflammatory factors and facilitate leukaemic blast expansion. **A** Nalm6 leukaemic spheroids cultured alone (left) and over a hLMC layer (right) after 8 days of culture. Details of peripheral (upper row) and internal (lower row) zones of leukaemia spheroids co-cultured with hLMCs are shown. The two cell types are distinguished by their morphology based on the staining of actin filaments with phalloidin (red) and the shape and size of the nuclei (DAPI; blue). Representative images of $n=4$ independent experiments. **B** Recovery of leukaemic cells in spheroids cultured in the presence (3D ALL cells + hLMCs) or absence (3D ALL cells) of leptomeningeal cells. Results represent the mean ± SEM of eight independent experiments (**$p \leq 0.01$, ***$p \leq 0.001$; Mann-Whitney U test). **C** Viability of leukaemic cells in spheroids cultured in the presence (3D ALL cells + hLMCs) or absence (3D ALL cells) of leptomeningeal cells. Results represent the mean ± SEM of 3–4 independent experiments. **D** Representative images of Ki67 expression in Nalm6 leukaemic cells growing within 3D spheroids in the presence or absence of phalloidin-positive hLMCs. **E** Percentage of $Ki67^+$ leukaemic cells in spheroids cultured alone or in the presence of hLMCs (mean ± SEM; $n=3$; **$p \leq 0.01$; Mann-Whitney U test). **F** Proliferation rate of Nalm6 and RS4;11 cells grown in 3D spheroids in the presence or absence of hLMCs for 8 days was determined by 7-AAD staining and analysed by flow cytometry. Mean ± SEM of proliferating cells ($S+G_2+M$ phases) from 3–4 independent experiments are shown (*$p \leq 0.05$; Mann-Whitney U test). **G** Cytokine and chemokine levels in the supernatant of co-cultures of leukaemia spheroids and hLMCs after 8 days. Results are expressed as increments relative to control hLMCs cultures and represent the mean ± SEM of 3–5 independent experiments ($^{\#}p \leq 0.05$, $^{\#\#}p \leq 0.01$ represent statistically significant differences in the comparison hLMCs vs. 3D Nalm6 cells + hLMCs; *$p \leq 0.05$, **$p \leq 0.01$ represent statistically significant differences in the comparison hLMCs vs. 3D Nalm6 cells; $^{\$}p \leq 0.05$, $^{\$\$}p \leq 0.01$ represent statistically significant differences in the comparison 3D Nalm6 vs. 3D Nalm6 cells + hLMCs (Mann-Whitney U test)

reduced or did not change the recovery of Nalm6 or RS4;11 leukaemic cells, respectively (Supplementary Fig. S6).

Using the same 3D co-culture system, we analysed the response of leptomeningeal cells to the presence of leukaemia cells. After 8 days, protein levels of pro-inflammatory cytokines, such as IL-6, TNFα, sTNF-RI or PTX3, were significantly increased in the supernatants of leukaemia spheroid-hLMC co-cultures compared to control hLMC cultures (Fig. 6G). In addition, the production of the chemokines CCL2, CXCL10 and CXCL12 was also significantly upregulated in hLMCs in response to the presence of leukaemia cells (Fig. 6G; Supplementary Fig. S7). In contrast, no pro-inflammatory response to the presence of BCP-ALL blasts was observed in hLMCs grown in conventional 2D co-cultures (Supplementary Fig. S8). Therefore, the interaction of leukaemic cell aggregates with leptomeningeal layers seem to favour the generation of a pro-inflammatory microenvironment that could promote tumour cell proliferation.

3.4 Development of chemoresistance mechanisms in meningeal leukaemic aggregates

We also investigated whether meningeal leukaemic aggregates could stimulate the development of chemoresistance mechanisms. After 48 h of exposure to high doses of the chemotherapy drug methotrexate (1 µM), flow cytometry analyses showed that the percentage of viable leukaemia ($AnexV^{-}IP^{-}$ $CD19^{+}$) cells was significantly higher in 3D BCP-ALL spheroids than in conventional 2D suspension cultures, suggesting that leukaemia cell aggregation per se confers protection against the effects of methotrexate (Fig. 7A, B). We then analysed whether the presence of leptomeningeal cells might confer additional protection to leukaemic cell aggregates against chemotherapy. As shown in Fig. 7C, significantly more viable leukaemic blasts were recovered from BCP-ALL spheroids co-cultured with hLMCs compared to leukaemic spheroids cultured alone (Fig. 7A, C). In order to know the possible mechanisms by which leptomeningeal cells are able to induce chemoresistance, the expression of different drug efflux ATP-binding cassette (ABC) transporters was analysed in BCP-ALL spheroids grown in the presence or absence of hLMCs. Interestingly, the expression of *ABCA2* and *ABCA3*, but not *ABCC1*, drug transporters was significantly upregulated in leukaemia cells when leptomeningeal cells were present (Fig. 7D). Therefore, upregulation of ABC pumps on leukaemia cells within meningeal aggregates could be one of the strategies developed by the tumour to evade chemotherapy.

4 Discussion

As previously described in brain autopsies from BCP-ALL patients [2], our results in a xenogeneic model show that the leptomeningeal infiltration of leukaemic blasts can appear diffusely distributed over the brain surface, although is more commonly found forming different sized cell aggregates, mainly in regions close to the major brain fissures. It is precisely at those locations where Smyth et al. [28] have recently described the presence of discontinuities in the arachnoid barrier, known as arachnoid cuff exit (ACE) points, which under basal and pathological conditions allow direct fluid and cell exchange between the dura mater and the SAS. The ACE points, created by bridging veins, are areas of high CSF flow [28, 29] and could represent regions through which leukaemic blasts could primarily enter and be retained at those locations. In support of this possibility, the authors described that ACE points are rich in laminin, whose interaction with VLA-6, which is expressed in leukaemic blasts, has been described to regulate leukaemic cell entry into the SAS [28, 30].

The study of the kinetics of BCP-ALL development showed that the onset of the meningeal metastasis occurred simultaneously with the invasion of other relevant organs such as the spleen. However, in the case of the CNS, leukaemic blasts, once infiltrated, are initially retained by a layer of ER-$TR7^{+}$ stromal cells present in the SAS which also hosts large numbers of myeloid cells (data not shown). Based on its location, the ER-TR7 expression and the abundance of myeloid cells, this layer may correspond to that recently described by several authors using intravital microscopy and molecular studies in different animal and human brains [6–8]. Møllgård et al. described this layer as a putative fourth meninge, the subarachnoid lymphatic-like membrane (SLYM), with protective barrier functions limiting the passage of molecules and cells between the internal and external compartments of the SAS and acting as a platform to monitor infections and inflammation by increasing the number of resident immune cells [7]. Further studies are needed to understand the characteristics of the ER-$TR7^{+}$ cell barrier encountered by leukaemic blasts in the early stages of CNS metastasis.

In more advanced stages of the disease, and after penetration of the ER-$TR7^{+}$ layer, the number of leukaemic blasts increases dramatically, forming large leukaemic aggregates supported by an open network of PDPN-positive leptomeningeal cells. In this context, PDPN has been described to regulate actomyosin contractility in ER-TR7-positive fibroblastic reticular cells found in secondary lymphoid organs. During inflammation, PDPN induces relaxation of the fibroblastic reticular cell network, allowing these cells to elongate and make room for expanding populations of

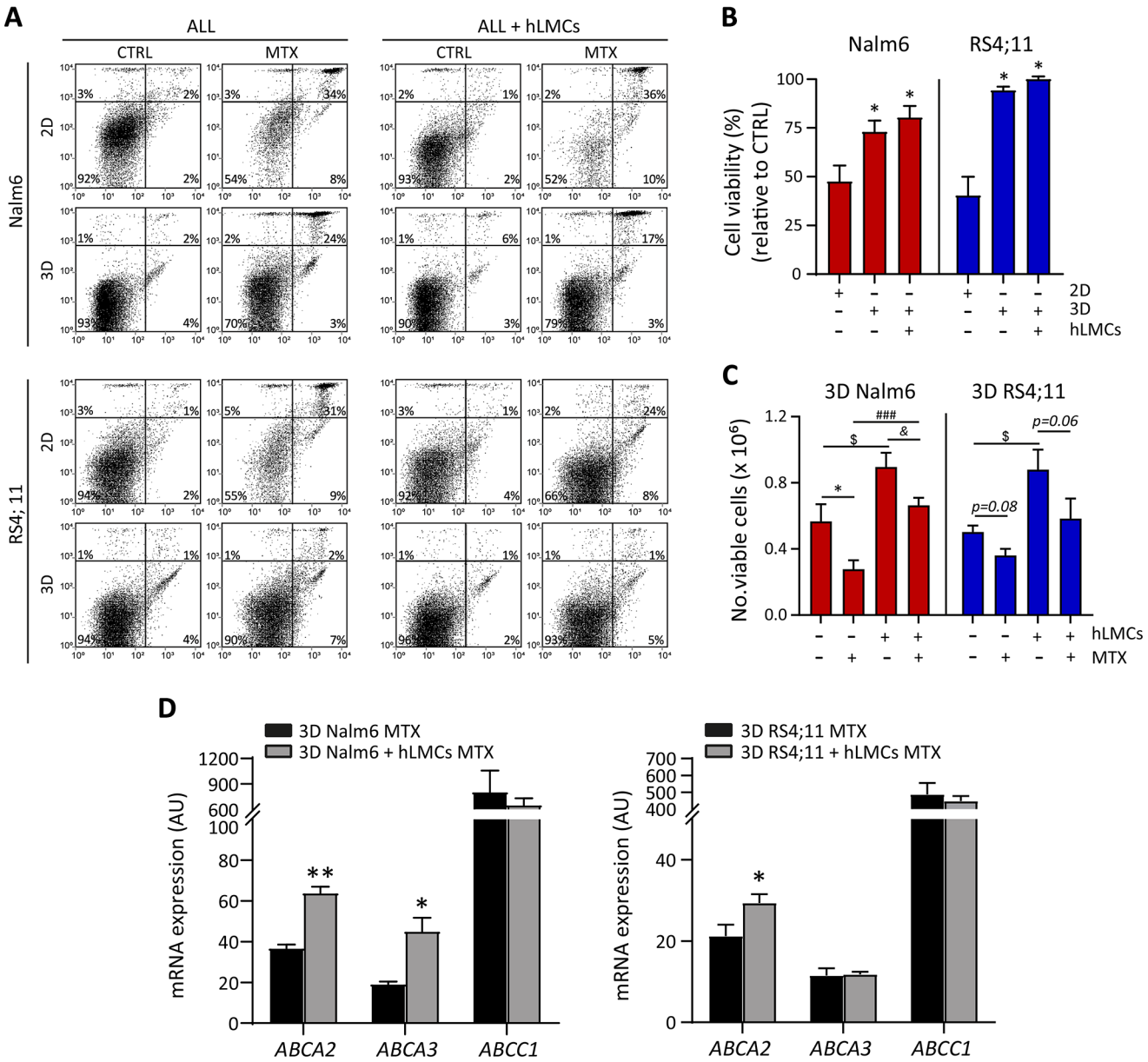

Fig. 7 Development of chemoresistance in leukaemic aggregates. **A** Representative annexin V/propidium iodide dot plots showing the viability of Nalm6 and RS4;11 leukaemic cells growing in 2D or 3D conditions and in the presence or absence of human leptomeningeal cells (hLMCs), after treatment with 1 μM methotrexate (MTX) for 48 h. **B** Percentage of viable leukaemic cells recovered from 2D cultures, and 3D spheroids cultured alone or co-cultured with hLMCs after treatment with MTX. Data from 3–5 independent experiments are expressed as the mean ± SEM of the relative cell viability compared to the corresponding untreated cultures (*$p \leq 0.05$ represent statistically significant differences respect to 2D cultures; Mann-Whitney U test). **C** Number of $CD19^+$ leukaemia cells recovered from 3D BCP-ALL spheroids cultured alone or with hLMCs and after exposure to 1 μM MTX. Mean ± SEM of 3–5 independent experiments is shown (*$p \leq 0.05$ represent statistically significant differences between MTX-treated and untreated cultures; $^{\$}p \leq 0.05$ represent statistically significant differences between untreated cultures in the presence or absence of hLMCs; $^{\#\#\#}p \leq 0.001$ represent statistically significant differences between MTX-treated cultures in the presence or absence of hLMCs; $^{\&}p \leq 0.05$ represent statistically significant differences between MTX-treated and untreated co-cultures with hLMCs; Mann-Whitney U test). **D** mRNA expression levels for ABC transporters in Nalm6 and RS4;11 leukaemic cells recovered from MTX-treated 3D spheroids co-cultured with or without hLMCs. Mean ± SEM of 3 independent experiments is shown (*$p \leq 0.05$, **$p \leq 0.01$; Mann-Whitney U test)

responding lymphocytes [31, 32], a situation that could also occur in the meningeal BCP-ALL aggregates exhibiting a pro-inflammatory profile. Likewise, Tamura et al. [33, 34] have also described in the bone marrow the presence of PDPN-expressing stromal cells that regulate the development and integrity of its primitive vasculature through the release of angiogenic factors contributing to bone marrow homeostasis.

On the other hand, these leukaemia-leptomeningeal cell aggregates are reminiscent of the pathogenic leptomeningeal B-cell clusters described in experimental autoimmune encephalomyelitis [35]. Pikor et al. reported that signals involved in the formation and maintenance of the meningeal B-cell clusters under chronic inflammatory conditions include pro-inflammatory cytokines and extracellular matrix components produced by, among others, meningeal cells [35]. In the case of BCP-ALL metastasis, the 3D spheroid co-culture model used in this study shows for the first time that the leukaemia-leptomeningeal cell aggregates also exhibit a higher expression of extracellular matrix components and adhesion molecules, as well as pro-inflammatory cytokines and chemokines. The increased production of IL-6, TNFα, sTNF-R1, PTX-3, CCL2 and CXCL10 could provide a suitable microenvironment for the maintenance of leukaemic blasts in the CNS, as has been described to occur in the bone marrow of ALL patients [20, 36–38]. The upregulated expression of the chemokines CXCL10 and CCL2 could also favour the arrival of new leukaemia cells contributing to increase the size of the meningeal aggregates. In this regard, CSF levels of CXCL10, CCL2 and TNFα were found to be significantly higher in ALL patients with CNS relapse and poor prognosis [39–41]. In addition, the increased production of CXCL12 by leptomeningeal cells in contact with the leukaemic spheroids may be particularly relevant for the survival of leukaemia blasts, as the CXCR4/CXCL12 axis has been described to play an important role in the biology of ALL, including CNS metastasis, and the treatment with a CXCR4 antagonist, which disrupts the adhesion of leukaemic cells to both bone marrow stroma and meningeal cells, renders tumour cells more susceptible to chemotherapy [24, 42–45]. Likewise, the increased expression of the integrins LFA-1 and VLA-4 as well as heparan sulphate in leukaemia cell spheroids suggests that the three-dimensional organisation achieved by leukaemia cells on the meningeal surface could favour the interaction between them and with the extracellular matrix and leptomeningeal cells expressing the corresponding receptors ICAM-1, VCAM-1 and CD44. Several evidences have pointed to a role for these integrins and the CD44 molecule in ALL cell adhesion to stromal cells and CNS colonisation, with particular involvement in mechanisms contributing to cancer cell survival and chemoresistance [46–50]. In this sense, it has been described that pharmacological downregulation of VCAM-1 in meningeal cells reduces ALL blast survival by inducing chemosensitivity [23].

Therefore, the meningeal aggregates appear to provide a permissive microenvironment for the recruitment, survival and maintenance of leukaemic blasts in the CNS, which is supported by the fact that the viability of leukaemic blasts recovered from CNS in the xenogeneic model was greater than 90% and similar to that of other organs such as the spleen or bone marrow. Nevertheless, in addition to the relevance of both pro-inflammatory factors and cell-to-cell/matrix interactions in promoting tumour survival as discussed above, it is worth noting that within the leukaemic meningeal nodules is possible to find blood vessels which could result from an angiogenic process, as suggested by the high levels of VEGF present in BCP-ALL brain metastases [51, 52]. Alternatively, leukaemia cells could interact with the abluminal surface of pre-existing vasculature and develop vessel co-option, as has been described in many solid tumours [53]. In any case, it is highly likely that this vascular supply present within the meningeal aggregates contributes notably to the maintenance of leukaemic cells and the progression of CNS metastases.

A relevant issue raised by the present study is that the progressive increase in the size of meningeal aggregates observed in the xenogeneic model is mainly due to leukaemic blast proliferation, as shown by the high number of dividing cells observed from the early stages of development of the leptomeningeal metastasis. Consistent with the in vivo results, the in vitro study using 3D spheroids shows that leptomeningeal cells induce the proliferation of leukaemic cells. These results are in apparent contrast to those reported by others [23] who have shown, using 2D suspension cultures, that interactions between leukaemia and meningeal cells reduce the tumour proliferation rate. In the current work, we have also co-cultured Nalm6 and RS4;11 cells with leptomeningeal cells in conventional 2D cultures and demonstrated that the expansion capacity of leukaemic cells is reduced or unaffected in this system. This therefore provides evidence that the three-dimensional organisation of the meningeal aggregates substantially modifies the behaviour of leukaemic cells and supports that 3D cell culture is a valuable tool also in ALL, offering significant advantages over traditional 2D cell culture.

Our current results show that the meningeal aggregates represent regions where leukaemia can actively divide and expand throughout the SAS, but also where it can develop chemoresistance. This capacity may be acquired in part through the increased cell-to-cell and cell-to-matrix interactions in the three-dimensional architectural configuration achieved in the leptomeningeal aggregates, as discussed above. Similar outcomes have been observed when acute myeloid leukaemia cells were cultured in a decellularised Wharton's jelly matrix [54]. The upregulated expression of ABC transporters, such as ABCA2 and ABCA3, is another chemoprotective mechanism seen in our leukaemia-leptomeningeal cell aggregates. Consistent with these results, Munch et al. [51] reported a significant upregulation of the expression of several ABC transporter family genes in BCP-ALL cells recovered from the SAS of xenografted mice compared to those obtained from the bone

marrow. Furthermore, an increased expression of ABCA2 and ABCA3 pumps has been described in leukaemic cells derived from paediatric T-ALL and B-ALL patients and associated with the development of minimal residual disease and relapse [55–57]. These data support the idea that these transporters, together with adhesion-derived signals, may be involved in the chemoresistance observed in leukaemia cells that form aggregates in contact with leptomeningeal cells.

5 Conclusions

The present work provides evidence for the dynamics of meningeal leukaemic aggregate formation and the contribution of leptomeningeal cells to this process. Meningeal leukaemic aggregates begin to organise in the early stages of the disease, concurrent with the detection of leukaemic invasion of other peripheral organs. Leptomeningeal cells strongly contribute to promoting leukaemic cell expansion in a three-dimensional microenvironment, contrary to what has been previously reported using two-dimensional approaches. Likewise, leptomeningeal cells, upon contact with leukaemia cells, generate a pro-inflammatory microenvironment, similar to that described in the leukaemic bone marrow, and also favour ABC transporter expression and the development of chemoresistance, which may result in treatment refractoriness and, potentially, relapse in the CNS.

Supplementary Information The online version contains supplementary material available at https://doi.org/10.1007/s13402-025-01043-y.

Acknowledgements We thank Dr. Ester Martín-Villar's lab for kindly providing anti-podoplanin antibody.

Author contributions POS performed experiments, acquired the data, analysed results and interpreted data; SGS, LHV, JV, EJ and RS performed experiments, acquired the data and analysed results; MR obtained patient samples and co-designed the study; IF co-designed the study and interpreted data; AVa co-designed the study, interpreted data and wrote, revised and edited the manuscript; LMFS and AVi conceived and designed the research, interpreted data and wrote, revised and edited the manuscript. All authors have read the manuscript and approved the final version for submission.

Funding This work was supported by grants PID2021-123068OB-I00/AEI/10.13039/501100011033/FEDER, UE (Spanish Ministry of Science and Innovation) RD21/0017/0010 and RD21/0017/0005 (Carlos III Health Institute, Madrid, Spain, co-financed by the European Union (NextGeneration EU)). POS was supported by a pre-doctoral fellowship (CT63/19-CT64/19) from the Complutense University. SGS is supported by a research contract from Carlos III Health Institute. LHV was supported by a doctoral fellowship (860-2019) from the Minciencias, Colombia.

Data availability No datasets were generated or analysed during the current study.

Declarations

Ethical approval and consent to participate All animal experimentation was conducted in accordance with the Spanish guidelines for care and use of laboratory animals and protocols approved by the Complutense University and Community of Madrid (PROEX 015/19; PROEX 204.2/22). BCP-ALL samples were provided by the Onco-Haematology Unit at Niño Jesús University Children's Hospital. Informed consent was provided according to the Declaration of Helsinki, and the study was approved by the Ethics Committee of Clinical Research at Niño Jesús Hospital (R-0009/22).

Competing interests The authors declare no competing interests.

References

1. M.T. Williams, Y.M. Yousafzai, A. Elder, K. Rehe, S. Bomken, L. Frishman-Levy, S. Tavor, P. Sinclair, K. Dormon, D. Masic, T. Perry, V.J. Weston, P. Kearns, H. Blair, L.J. Russell, O. Heidenreich, J.A. Irving, S. Izraeli, J. Vormoor, G.J. Graham, C. Halsey, The ability to cross the blood-cerebrospinal fluid barrier is a generic property of acute lymphoblastic leukemia blasts. Blood. **127**(16), 1998–2006 (2016). https://doi.org/10.1182/blood-2015-08-665034
2. R.A. Price, W.W. Johnson, The central nervous system in childhood leukemia. I. The arachnoid. Cancer. **31**(3), 520–533 (1973). https://doi.org/10.1002/1097-0142(197303)31:3%3C520::aid-cncr2820310306%3E3.0.co;2-2
3. Y.T. Cheung, N.D. Sabin, W.E. Reddick, D. Bhojwani, W. Liu, T.M. Brinkman, J.O. Glass, S.N. Hwang, D. Srivastava, C.H. Pui, L.L. Robison, M.M. Hudson, K.R. Krull, Leukoencephalopathy and long-term neurobehavioural, neurocognitive, and brain imaging outcomes in survivors of childhood acute lymphoblastic leukaemia treated with chemotherapy: a longitudinal analysis. Lancet Haematol. **3**(10), e456–e466 (2016). https://doi.org/10.1016/S2352-3026(16)30110-7
4. N.S. Phillips, K.L. Stratton, A.M. Williams, T. Ahles, K.K. Ness, H.J. Cohen, K. Edelstein, Y. Yasui, K. Oeffinger, E.J. Chow, R.M. Howell, L.L. Robison, G.T. Armstrong, W.M. Leisenring, K.R. Krull, Late-onset cognitive impairment and modifiable risk factors in adult Childhood Cancer survivors. JAMA Netw. Open. **6**(5), e2316077 (2023). https://doi.org/10.1001/jamanetworkopen.2023.16077
5. W.A. Mills, M.A. Coburn, U.B. Eyo, The emergence of the calvarial hematopoietic niche in health and disease. Immunol. Rev. **311**(1), 26–38 (2022). https://doi.org/10.1111/imr.13120

6. R. Pietila, F. Del Gaudio, L. He, E. Vazquez-Liebanas, M. Vanlandewijck, L. Muhl, G. Mocci, K.D. Bjornholm, C. Lindblad, A. Fletcher-Sandersjoo, M. Svensson, E.P. Thelin, J. Liu, A.J. van Voorden, M. Torres, S. Antila, L. Xin, H. Karlstrom, J. Storm-Mathisen, L.H. Bergersen, A. Moggio, E.M. Hansson, M.H. Ulvmar, P. Nilsson, T. Makinen, M. Andaloussi Mae, K. Alitalo, S.T. Proulx, B. Engelhardt, D.M. McDonald, U. Lendahl, J. Andrae, C. Betsholtz, Molecular anatomy of adult mouse leptomeninges. Neuron. **111**(23), 3745–3764e3747 (2023). https://doi.org/10.1016/j.neuron.2023.09.002
7. K. Mollgard, F.R.M. Beinlich, P. Kusk, L.M. Miyakoshi, C. Delle, V. Pla, N.L. Hauglund, T. Esmail, M.K. Rasmussen, R.S. Gomolka, Y. Mori, M. Nedergaard, A mesothelium divides the subarachnoid space into functional compartments. Science. **379**(6627), 84–88 (2023). https://doi.org/10.1126/science.adc8810
8. J.A. Mapunda, J. Pareja, M. Vladymyrov, E. Bouillet, P. Helie, P. Pleskac, S. Barcos, J. Andrae, D. Vestweber, D.M. McDonald, C. Betsholtz, U. Deutsch, S.T. Proulx, B. Engelhardt, VE-cadherin in arachnoid and pia mater cells serves as a suitable landmark for in vivo imaging of CNS immune surveillance and inflammation. Nat. Commun. **14**(1), 5837 (2023). https://doi.org/10.1038/s41467-023-41580-4
9. C. Niu, J. Yu, T. Zou, Y. Lu, L. Deng, H. Yun, C.Y. Si, X. Wu, H. Jiang, T. Guo, M. Wu, T. Kan, J. Feng, C. Yuan, X. Yang, Q. Cheng, J. Dong, Q. Wang, J. Zhang, Identification of hematopoietic stem cells residing in the meninges of adult mice at steady state. Cell. Rep. **41**(6), 111592 (2022). https://doi.org/10.1016/j.celrep.2022.111592
10. S. Brioschi, W.L. Wang, V. Peng, M. Wang, I. Shchukina, Z.J. Greenberg, J.K. Bando, N. Jaeger, R.S. Czepielewski, A. Swain, D.A. Mogilenko, W.L. Beatty, P. Bayguinov, J.A.J. Fitzpatrick, L.G. Schuettpelz, C.C. Fronick, I. Smirnov, J. Kipnis, V.S. Shapiro, G.F. Wu, S. Gilfillan, M. Cella, M.N. Artyomov, S.H. Kleinstein, M. Colonna, Heterogeneity of meningeal B cells reveals a lymphopoietic niche at the CNS borders. Science. **373**(6553) (2021). https://doi.org/10.1126/science.abf9277
11. V. Ramaglia, A. Florescu, M. Zuo, S. Sheikh-Mohamed, J.L. Gommerman, Stromal cell-mediated coordination of Immune Cell Recruitment, Retention, and function in brain-adjacent regions. J. Immunol. **206**(2), 282–291 (2021). https://doi.org/10.4049/jimmunol.2000833
12. J. Cupovic, L. Onder, C. Gil-Cruz, E. Weiler, S. Caviezel-Firner, C. Perez-Shibayama, T. Rulicke, I. Bechmann, B. Ludewig, Central nervous system stromal cells control local CD8(+) T cell responses during Virus-Induced Neuroinflammation. Immunity. **44**(3), 622–633 (2016). https://doi.org/10.1016/j.immuni.2015.12.022
13. R. Watanabe, M. Kakizaki, Y. Ikehara, A. Togayachi, Formation of fibroblastic reticular network in the brain after infection with neurovirulent murine coronavirus. Neuropathology. **36**(6), 513–526 (2016). https://doi.org/10.1111/neup.12302
14. E.H. Wilson, T.H. Harris, P. Mrass, B. John, E.D. Tait, G.F. Wu, M. Pepper, E.J. Wherry, F. Dzierzinski, D. Roos, P.G. Haydon, T.M. Laufer, W. Weninger, C.A. Hunter, Behavior of parasite-specific effector CD8+T cells in the brain and visualization of a kinesis-associated system of reticular fibers. Immunity. **30**(2), 300–311 (2009). https://doi.org/10.1016/j.immuni.2008.12.013
15. O.W. Howell, C.A. Reeves, R. Nicholas, D. Carassiti, B. Radotra, S.M. Gentleman, B. Serafini, F. Aloisi, F. Roncaroli, R. Magliozzi, R. Reynolds, Meningeal inflammation is widespread and linked to cortical pathology in multiple sclerosis. Brain. **134**(9), 2755–2771 (2011). https://doi.org/10.1093/brain/awr182
16. R.J. Bevan, R. Evans, L. Griffiths, L.M. Watkins, M.I. Rees, R. Magliozzi, I. Allen, G. McDonnell, R. Kee, M. Naughton, D.C. Fitzgerald, R. Reynolds, J.W. Neal, O.W. Howell, Meningeal inflammation and cortical demyelination in acute multiple sclerosis. Ann. Neurol. **84**(6), 829–842 (2018). https://doi.org/10.1002/ana.25365
17. L.B. Thomas, Pathology of leukemia in the brain and meninges: postmortem studies of patients with acute leukemia and of mice given inoculations of L1210 leukemia. Cancer Res. **25**(9), 1555–1571 (1965)
18. M. Lorger, B. Felding-Habermann, Capturing changes in the brain microenvironment during initial steps of breast cancer brain metastasis. Am. J. Pathol. **176**(6), 2958–2971 (2010). https://doi.org/10.2353/ajpath.2010.090838
19. A. Sanchez-Aguilera, S. Mendez-Ferrer, The hematopoietic stem-cell niche in health and leukemia. Cell. Mol. Life Sci. **74**(4), 579–590 (2017). https://doi.org/10.1007/s00018-016-2306-y
20. E. Dander, C. Palmi, G. D'Amico, G. Cazzaniga, The bone Marrow Niche in B-Cell Acute Lymphoblastic Leukemia: the role of Microenvironment from Pre-leukemia to overt leukemia. Int. J. Mol. Sci. **22**(9), 4426 (2021). https://doi.org/10.3390/ijms22094426
21. S.M. Akers, S.L. Rellick, J.E. Fortney, L.F. Gibson, Cellular elements of the subarachnoid space promote ALL survival during chemotherapy. Leuk. Res. **35**(6), 705–711 (2011). https://doi.org/10.1016/j.leukres.2010.12.031
22. P. Basile, L.M. Jonart, M. Ebadi, K. Johnson, M. Kerfeld, P.M. Gordon, The meninges enhance leukaemia survival in cerebral spinal fluid. Br. J. Haematol. **189**(3), 513–517 (2020). https://doi.org/10.1111/bjh.16270
23. L.M. Jonart, M. Ebadi, P. Basile, K. Johnson, J. Makori, P.M. Gordon, Disrupting the leukemia niche in the central nervous system attenuates leukemia chemoresistance. Haematologica. **105**(8), 2130–2140 (2020). https://doi.org/10.3324/haematol.2019.230334
24. L.M. Jonart, J. Ostergaard, A. Brooks, G. Fitzpatrick, L. Chen, P.M. Gordon, CXCR4 antagonists disrupt leukaemia-meningeal cell adhesion and attenuate chemoresistance. Br. J. Haematol. **201**(3), 459–469 (2023). https://doi.org/10.1111/bjh.18607
25. F.G.S.A. Gandarillas, N. Benito, C. Gamallo, M. Quintanilla, Induction of PA2.26, a cell-surface antigen expressed by active fibroblasts, in mouse epidermal keratinocytes during carcinogenesis. Mol. Carcinog. **20**(1), 10–18 (1997). https://doi.org/10.1002/(sici)1098-2744(199709)20:1%3C10::aid-mc3%3E3.0.co;2-m
26. V. Pla, S. Bitsika, M.J. Giannetto, A. Ladron-de-Guevara, D. Gahn-Martinez, Y. Mori, M. Nedergaard, K. Mollgard, Structural characterization of SLYM-a 4th meningeal membrane. Fluids Barriers CNS. **20**(1), 93 (2023). https://doi.org/10.1186/s12987-023-00500-w
27. R.C. Sterner, R.M. Sterner, CAR-T cell therapy: current limitations and potential strategies. Blood Cancer J. **11**(4), 69 (2021). https://doi.org/10.1038/s41408-021-00459-7
28. L.C.D. Smyth, D. Xu, S.V. Okar, T. Dykstra, J. Rustenhoven, Z. Papadopoulos, K. Bhasiin, M.W. Kim, A. Drieu, T. Mamuladze, S. Blackburn, X. Gu, M.I. Gaitan, G. Nair, S.E. Storck, S. Du, M.A. White, P. Bayguinov, I. Smirnov, K. Dikranian, D.S. Reich, J. Kipnis, Identification of direct connections between the dura and the brain. Nature. **627**(8002), 165–173 (2024). https://doi.org/10.1038/s41586-023-06993-7
29. X. Chen, X. Liu, S. Koundal, R. Elkin, X. Zhu, B. Monte, F. Xu, F. Dai, M. Pedram, H. Lee, J. Kipnis, A. Tannenbaum, W.E. Van Nostrand, H. Benveniste, Cerebral amyloid angiopathy is associated with glymphatic transport reduction and time-delayed solute drainage along the neck arteries. Nat. Aging. **2**(3), 214–223 (2022). https://doi.org/10.1038/s43587-022-00181-4
30. H. Yao, T.T. Price, G. Cantelli, B. Ngo, M.J. Warner, L. Olivere, S.M. Ridge, E.M. Jablonski, J. Therrien, S. Tannheimer, C.M. McCall, A. Chenn, D.A. Sipkins, Leukaemia hijacks a neural mechanism to invade the central nervous system. Nature.

560(7716), 55–60 (2018). https://doi.org/10.1038/s41586-018-0342-5
31. S.E. Acton, A.J. Farrugia, J.L. Astarita, D. Mourao-Sa, R.P. Jenkins, E. Nye, S. Hooper, J. van Blijswijk, N.C. Rogers, K.J. Snelgrove, I. Rosewell, L.F. Moita, G. Stamp, S.J. Turley, E. Sahai, Reis E Sousa, dendritic cells control fibroblastic reticular network tension and lymph node expansion. Nature. **514**(7523), 498–502 (2014). https://doi.org/10.1038/nature13814
32. J.L. Astarita, V. Cremasco, J. Fu, M.C. Darnell, J.R. Peck, J.M. Nieves-Bonilla, K. Song, Y. Kondo, M.C. Woodruff, A. Gogineni, L. Onder, B. Ludewig, R.M. Weimer, M.C. Carroll, D.J. Mooney, L. Xia, S.J. Turley, The CLEC-2-podoplanin axis controls the contractility of fibroblastic reticular cells and lymph node microarchitecture. Nat. Immunol. **16**(1), 75–84 (2015). https://doi.org/10.1038/ni.3035
33. S. Tamura, K. Suzuki-Inoue, N. Tsukiji, T. Shirai, T. Sasaki, M. Osada, K. Satoh, Y. Ozaki, Podoplanin-positive periarteriolar stromal cells promote megakaryocyte growth and proplatelet formation in mice by CLEC-2. Blood. **127**(13), 1701–1710 (2016). https://doi.org/10.1182/blood-2015-08-663708
34. S. Tamura, M. Mukaide, Y. Katsuragi, W. Fujii, K. Odaira, N. Suzuki, N. Tsukiji, S. Okamoto, A. Suzuki, T. Kanematsu, A. Katsumi, A. Takagi, K. Ikeda, J. Ueyama, M. Hirayama, K. Suzuki-Inoue, T. Matsushita, T. Kojima, F. Hayakawa, Periosteum-derived podoplanin-expressing stromal cells regulate nascent vascularization during epiphyseal marrow development. J. Biol. Chem. **298**(5), 101833 (2022). https://doi.org/10.1016/j.jbc.2022.101833
35. N.B. Pikor, J.L. Astarita, L. Summers-Deluca, G. Galicia, J. Qu, L.A. Ward, S. Armstrong, C.X. Dominguez, D. Malhotra, B. Heiden, R. Kay, V. Castanov, H. Touil, L. Boon, P. O'Connor, A. Bar-Or, A. Prat, V. Ramaglia, S. Ludwin, S.J. Turley, J.L. Gommerman, Integration of Th17- and lymphotoxin-derived signals initiates meningeal-resident stromal cell remodeling to Propagate Neuroinflammation. Immunity. **43**(6), 1160–1173 (2015). https://doi.org/10.1016/j.immuni.2015.11.010
36. A. Vilchis-Ordonez, A. Contreras-Quiroz, E. Vadillo, E. Dorantes-Acosta, A. Reyes-Lopez, H.M. Venegas-Vazquez, H. Mayani, V. Ortiz-Navarrete, B. Lopez-Martinez, R. Pelayo, Bone Marrow Cells in Acute Lymphoblastic Leukemia Create a Proinflammatory Microenvironment Influencing Normal Hematopoietic Differentiation Fates. Biomed Res Int. **2015**(1), 386165 (2015). https://doi.org/10.1155/2015/386165
37. A. Entrena, A. Varas, M. Vazquez, G.J. Melen, L.M. Fernandez-Sevilla, J. Garcia-Castro, M. Ramirez, A.G. Zapata, A. Vicente, Mesenchymal stem cells derived from low risk acute lymphoblastic leukemia patients promote NK cell antitumor activity. Cancer Lett. **363**(2), 156–165 (2015). https://doi.org/10.1016/j.canlet.2015.04.012
38. L. Beneforti, E. Dander, S. Bresolin, C. Bueno, D. Acunzo, M. Bertagna, A. Ford, B. Gentner, G.T. Kronnie, P. Vergani, P. Menendez, A. Biondi, G. D'Amico, C. Palmi, G. Cazzaniga, Proinflammatory cytokines favor the emergence of ETV6-RUNX1-positive pre-leukemic cells in a model of mesenchymal niche. Br. J. Haematol. **190**(2), 262–273 (2020). https://doi.org/10.1111/bjh.16523
39. A.M. Gomez, C. Martinez, M. Gonzalez, A. Luque, G.J. Melen, J. Martinez, S. Hortelano, A. Lassaletta, L. Madero, M. Ramirez, Chemokines and relapses in childhood acute lymphoblastic leukemia: a role in migration and in resistance to antileukemic drugs. Blood Cells Mol. Dis. **55**(3), 220–227 (2015). https://doi.org/10.1016/j.bcmd.2015.07.001
40. M.Y. Si, Z.C. Fan, Y.Z. Li, X.L. Chang, Q.D. Xie, X.Y. Jiao, The prognostic significance of serum and cerebrospinal fluid MMP-9, CCL2 and sVCAM-1 in leukemia CNS metastasis. J. Neurooncol. **122**(2), 229–244 (2015). https://doi.org/10.1007/s11060-014-1707-8
41. J.C. Jaime-Perez, C.M. Gamboa-Alonso, R.A. Jimenez-Castillo, L.J. Lopez-Silva, M.A. Pinzon-Uresti, A. Gomez-De Leon, D. Gomez-Almaguer, TNF-alpha increases in the CSF of children with acute lymphoblastic leukemia before CNS relapse. Blood Cells Mol. Dis. **63**, 27–31 (2017). https://doi.org/10.1016/j.bcmd.2016.12.011
42. L. Su, Z. Hu, Y.G. Yang, Role of CXCR4 in the progression and therapy of acute leukaemia. Cell. Prolif. **54**(7), e13076 (2021). https://doi.org/10.1111/cpr.13076
43. J. Juarez, A. Dela Pena, R. Baraz, J. Hewson, M. Khoo, A. Cisterne, S. Fricker, N. Fujii, K.F. Bradstock, L.J. Bendall, CXCR4 antagonists mobilize childhood acute lymphoblastic leukemia cells into the peripheral blood and inhibit engraftment. Leukemia. **21**(6), 1249–1257 (2007). https://doi.org/10.1038/sj.leu.2404684
44. R. Crazzolara, A. Kreczy, G. Mann, A. Heitger, G. Eibl, F.M. Fink, R. Mohle, B. Meister, High expression of the chemokine receptor CXCR4 predicts extramedullary organ infiltration in childhood acute lymphoblastic leukaemia. Br. J. Haematol. **115**(3), 545–553 (2001). https://doi.org/10.1046/j.1365-2141.2001.03164.x
45. T.R. Jost, C. Borga, E. Radaelli, A. Romagnani, L. Perruzza, L. Omodho, G. Cazzaniga, A. Biondi, S. Indraccolo, M. Thelen, G. Te Kronnie, F. Grassi, Role of CXCR4-mediated bone marrow colonization in CNS infiltration by T cell acute lymphoblastic leukemia. J. Leukoc. Biol. **99**(6), 1077–1087 (2016). https://doi.org/10.1189/jlb.5MA0915-394R
46. L.M. Fernandez-Sevilla, J. Valencia, M.A. Flores-Villalobos, A. Gonzalez-Murillo, R. Sacedon, E. Jimenez, M. Ramirez, A. Varas, A. Vicente, The choroid plexus stroma constitutes a sanctuary for paediatric B-cell precursor acute lymphoblastic leukaemia in the central nervous system. J. Pathol. **252**(2), 189–200 (2020). https://doi.org/10.1002/path.5510
47. R. Jacamo, Y. Chen, Z. Wang, W. Ma, M. Zhang, E.L. Spaeth, Y. Wang, V.L. Battula, P.Y. Mak, K. Schallmoser, P. Ruvolo, W.D. Schober, E.J. Shpall, M.H. Nguyen, D. Strunk, C.E. Bueso-Ramos, S. Konoplev, R.E. Davis, M. Konopleva, M. Andreeff, Reciprocal leukemia-stroma VCAM-1/VLA-4-dependent activation of NF-kappaB mediates chemoresistance. Blood. **123**(17), 2691–2702 (2014). https://doi.org/10.1182/blood-2013-06-511527
48. R.E. Mudry, J.E. Fortney, T. York, B.M. Hall, L.F. Gibson, Stromal cells regulate survival of B-lineage leukemic cells during chemotherapy. Blood. **96**(5), 1926–1932 (2000)
49. S. Wu, Y. Tan, F. Li, Y. Han, S. Zhang, X. Lin, CD44: a cancer stem cell marker and therapeutic target in leukemia treatment. Front. Immunol. **15**, 1354992 (2024). https://doi.org/10.3389/fimmu.2024.1354992
50. B. Scharff, S. Modvig, H.V. Marquart, C. Christensen, Integrin-mediated adhesion and chemoresistance of Acute Lymphoblastic Leukemia cells residing in the bone marrow or the Central Nervous System. Front. Oncol. **10**, 775 (2020). https://doi.org/10.3389/fonc.2020.00775
51. V. Munch, L. Trentin, J. Herzig, S. Demir, F. Seyfried, J.M. Kraus, H.A. Kestler, R. Kohler, T.F.E. Barth, G. Te Kronnie, K.M. Debatin, L.H. Meyer, Central nervous system involvement in acute lymphoblastic leukemia is mediated by vascular endothelial growth factor. Blood. **130**(5), 643–654 (2017). https://doi.org/10.1182/blood-2017-03-769315
52. L.M. Fernandez-Sevilla, J. Valencia, P. Ortiz-Sanchez, A. Fraile-Ramos, P. Zuluaga, E. Jimenez, R. Sacedon, M.V. Martinez-Sanchez, J. Jazbec, M. Debeljak, B. Fedders, M. Stanulla, D. Schewe, G. Cario, A. Minguela, M. Ramirez, A. Varas, A. Vicente, High BMP4 expression in low/intermediate risk BCP-ALL identifies children with poor outcomes. Blood. **139**(22), 3303–3313 (2022). https://doi.org/10.1182/blood.2021013506

53. E.A. Kuczynski, P.B. Vermeulen, F. Pezzella, R.S. Kerbel, A.R. Reynolds, Vessel co-option in cancer. Nat. Rev. Clin. Oncol. **16**(8), 469–493 (2019). https://doi.org/10.1038/s41571-019-0181-9
54. D. Li, T.L. Lin, B. Lipe, R.A. Hopkins, H. Shinogle, O.S. Aljitawi, A novel extracellular matrix-based leukemia model supports leukemia cells with stem cell-like characteristics. Leuk. Res. **72**, 105–112 (2018). https://doi.org/10.1016/j.leukres.2018.08.012
55. S. Rahgozar, A. Moafi, M. Abedi, E.G.M. Entezar, J. Moshtaghian, K. Ghaedi, A. Esmaeili, F. Montazeri, mRNA expression profile of multidrug-resistant genes in acute lymphoblastic leukemia of children, a prognostic value for ABCA3 and ABCA2. Cancer Biol. Ther. **15**(1), 35–41 (2014). https://doi.org/10.4161/cbt.26603
56. N. Aberuyi, S. Rahgozar, Z. Khosravi Dehaghi, A. Moafi, A. Masotti, A. Paolini, The translational expression of ABCA2 and ABCA3 is a strong prognostic biomarker for multidrug resistance in pediatric acute lymphoblastic leukemia. Onco Targets Ther. **10**, 3373–3380 (2017). https://doi.org/10.2147/OTT.S140488
57. N. Aberuyi, S. Rahgozar, E. Pourabutaleb, K. Ghaedi, Selective dysregulation of ABC transporters in methotrexate-resistant leukemia T-cells can confer cross-resistance to cytarabine, vincristine and dexamethasone, but not doxorubicin. Curr. Res. Transl Med. **69**(1), 103269 (2021). https://doi.org/10.1016/j.retram.2020.09.003

Authors and Affiliations

Paula Ortiz-Sánchez[1] · Sara González-Soto[1,2] · Luz H. Villamizar[1] · Jaris Valencia[1,3] · Eva Jiménez[1,3] · Rosa Sacedón[1,3] · Manuel Ramírez[4,5] · Isabel Fariñas[6] · Alberto Varas[1,3] · Lidia M. Fernández-Sevilla[3,7] · Ángeles Vicente[1,2]

✉ Alberto Varas
avaras@ucm.es

✉ Lidia M. Fernández-Sevilla
lidia.martinez@urjc.es

✉ Ángeles Vicente
avicente@ucm.es

[1] Department of Cell Biology, Faculty of Medicine, Complutense University, Madrid, Spain

[2] Health Research Institute Hospital 12 de Octubre (Imas12), Madrid, Spain

[3] Health Research Institute Hospital Clínico San Carlos (IdISSC), Madrid, Spain

[4] Department of Paediatric Haematology and Oncology, Advanced Therapies Unit, Niño Jesús University Children's Hospital, Madrid, Spain

[5] Health Research Institute Hospital La Princesa, Madrid, Spain

[6] Biomedical Research Network on Neurodegenerative Diseases (CIBERNED), Department of Cell Biology and Biotechnology and Biomedicine Institute (BioTecMed), University of Valencia, Valencia, Spain

[7] Department of Basic Health Sciences, Faculty of Health Sciences, University Rey Juan Carlos, Alcorcón, Spain